Dalton Transactions

Accepted Manuscript

ROYAL SOCIETY OF CHEMISTRY

www.rsc.org/dalton

Journal Name

ARTICLE

High Pressure Behaviour and Elastic Properties of a Dense Inorganic-Organic Framework

[Received 00th January 20xx, Accepted 00th January 20xx

DOI: 10.1039/x0xx00000x

www.rsc.org/

Guoqiang Feng,[‡a,b] Xingxing Jiang,[‡c] Wenjuan Wei,[a] Pifu Gong,[c] Lei Kang,[c] Zhihua Li,[a] Yanchun Li,[d] Xiaodong Li,[d] Xiang Wu,[e] Zheshuai Lin,*[c] Wei Li,*[a] Peixiang Lu[a,f]

The high pressure behaviour of a cubic dense inorganic–organic framework $[DABCOH_2^{2+}][K(ClO_4)_3]$ ($DABCOH_2^{2+}$ = diazabicyclo[2.2.2]octane-1,4-diium) has been systematically studied *via* synchrotron X-ray powder diffraction, over the range of 0-3.12 GPa. Framework $[DABCOH_2^{2+}][K(ClO_4)_3]$ shows a more rigid response, with bulk modulus of 30(1) GPa and axial compressibility of $7.6(4) \times 10^{-3}$ GPa^{-1}, compared with ZIF-8 and dense hybrid solar cell perovskite $CH_3NH_3PbI_3$. Density functional theory calculations reveal the structural change in $[DABCOH_2^{2+}][K(ClO_4)_3]$ is attributed to the contraction of the KO_{12} polyhedra, which consequently results in the rotation of the perchlorate linkers and synergistic movement of the $DABCOH_2^{2+}$ guest. Further extensive theoretical calculations of full elastic tensors give full mapping of the Young's moduli, shear moduli and Poisson's ratios of $[DABCOH_2^{2+}][K(ClO_4)_3]$, which are in the range of 31.6-36.6, 12.3-14.6 GPa and 0.2-0.32, respectively. The Young's and shear moduli of $[DABCOH_2^{2+}][K(ClO_4)_3]$ are larger than those from cubic MOF-5, ZIF-8 and $CH_3NH_3PbI_3$. In addition, the narrow range of Poisson's ratios in $[DABCOH_2^{2+}][K(ClO_4)_3]$ indicates its very isotropic nature in response to biaxial stress.

Introduction

Porous hybrid inorganic-organic framework materials have been studied intensively in chemistry, physics, and material science due to their potential applications in carbon capture, gas separation, catalysis, drug delivery and sensoring.[1,2] Recently, considerable efforts have been dedicated to investigating dense inorganic-organic frameworks since they show fascinating physical properties, such as semiconductivity, ferromagnetism, ferroelectricity and multiferroicity, which are dominated by traditional inorganic materials. For example, a family of dense hybrid perovskites, $[AmineH^+][MX_3]$ (Amine = methylammonium or formadinium, M = Sn or Pb, X = Cl, Br or I), have been reported to function as light harvesters in solid state sensitised solar cell devices with impressive efficiency values about 20%.[3,4] Another dense framework, $[NH_4][Zn(HCOO)_3]$ has been shown to be a striking multifunctional material with combined ferroelectricity, negative thermal expansion and negative linear compressibility.[5-7] However, there is a major lack of knowledge about their fundamental mechanical properties, which apparently could delay the development of driving these promising materials towards practical applications. In contrast, the mechanical properties of many porous frameworks (i.e. MOF-5,[8,9] ZIF-8,[10,11]) have been extensively studied, and significant information about their elasticity, plasticity, and structural stability upon stress have been reported. To attract more attention on dense hybrid frameworks and motivate more efforts dedicated to this important area, herein we focus our interest in the mechanical properties of a dense framework, $[DABCOH_2^{2+}][K(ClO_4)_3]$. In this work, we studied the high-pressure behaviour and elastic properties of dense framework $[DABCOH_2^{2+}][K(ClO_4)_3]$ *via* high-pressure synchrotron powder X-ray diffraction (PXRD) and first-principles calculation approaches. We demonstrate that the general rigid behaviour and isotropic elastic properties of this cubic hybrid framework can be ascribed to its underlying structural nature which mainly are dominated by the isotropic KO_{12} coordination polyhedra, rigid perchlorate linkers and synergistic interactions between the $DABCOH_2^{2+}$ and the $[K(ClO_4)_3]^{2-}$ framework.

[a]*School of Physics and Wuhan National High Magnetic Field Center, Huazhong University of Science and Technology, Wuhan 430074, China. E-mail: wl276@hust.edu.cn*
[b]*Department of Physics and Mechanical & Electrical Engineering, Hubei University of Education, Wuhan 430205, China*
[c]*Center for Crystal R&D, Key Lab of Functional Crystals and Laser Technology of Chinese Academy of Sciences, Technical Institute of Physics and Chemistry, Chinese Academy of Sciences, Beijing 100190, China. E-mail: zslin@mail.ipc.ac.cn*
[d]*Beijing Synchrotron Radiation Facility, Institute of High Energy Physics, Chinese Academy of Sciences, Beijing 100049, China*
[e]*School of Earth and Space Sciences, Peking University, Beijing 100871, China*
[f]*Laboratory for Optical Information Technology,Wuhan Institute of Technology, Wuhan 430205, China*
‡*These authors contributed equally to this work.*

Experimental

Synthesis

All chemicals and solvents were of reagent grade and used as received. The compound was prepared according to a previously published method.[12] In short, a solution ($KClO_4$: 1 mmol in 10 ml H_2O) was added slowly into 10 ml of an aqueous solution of DABCO (1 mmol) and $HClO_4$ (2 mmol). Blocky colourless crystals were formed from the solution by slow evaporation after a few days.

High-pressure synchrotron X-ray diffraction

The high-pressure XRD experiments were performed at the 4W2 beam line of Beijing Synchrotron Radiation Facility (BSRF). The X-ray beam with the wavelength of 0.61992 Å was focused into a 36 × 12 μm^2 spot using Kirkpatrick–Baez mirrors. The hydrostatic pressure was exerted by the systematic diamond anvil cells (DACs) with the culet diameter of 400 μm. The samples in well ground powder form were placed in a hole of about 120 μm diameter in a pre-indented stainless steel gasket with the thickness about 40 μm. The silicone oil was adopted to act as the pressure-transmitting medium and ruby chips were placed for pressure calibration by measuring the fluorescence shift as the function of pressure.[13] The diffraction patterns were recorded by a Pilatus 2M detector and integrated with the FIT2D software package.[14] The cell parameters under different pressure were refined by Rietveld method using general structure analysis system (GSAS) program.[15]

First-principles calculation

The first-principles calculations were performed by CASTEP,[16,17] a total energy package based on plane-wave pseudopotential density functional theory (DFT).[17] The functionals developed by Ceperley, Alder, Perdew and Zunger (CA-PZ) in local density approximation (LDA)[18] were adopted to describe the exchange-correlation energy. Optimized ultrasoft pseudopotentials [19] were adopted to model the effective interaction between the valence electrons and atom cores, which allow us to adopt a relatively small plane-wave basis set without compromising the computational accuracy. Kinetic energy cutoff 400 eV and Monkhorst-pack[20] k-point mesh spanning less than 0.04 $Å^{-1}$ were chosen.

For the elastic constant calculation, the crystal structure at 0 GPa was firstly optimized using Broyden–Fletcher–Goldfarb–Shanno (BFGS) minimization scheme.[21] And in the geometry optimization, both cell parameters and atomic positions were relaxed, and the convergence criterions for energy, maximum force, maximum stress and maximum displacement were set as 10^{-5} eV/atom, 0.03 eV, 0.05 GPa and 0.001 Å, respectively. Based on the above optimised crystal structure at 0 GPa, the elastic constants were calculated by the finite-strain method,[22] in which, the maximum strain amplitude and the number of steps for each strain were set as 0.003 and 3 steps, respectively. After obtaining the calculated elastic constants, the analyses of Young's modulus, shear modulus and Poisson's ratio were performed using the EIAM program.[23]

To further elucidate the microscopic changes of the lattice structure under pressure, the atomic coordinates in 0, 1.59 and 3.12 GPa were refined by first-principles geometry optimization. In this geometry optimization, the cell parameters under variable pressures were fixed at the experimental values and were not optimized, and only the atomic coordinates at each pressure were optimized.

Results and Discussion

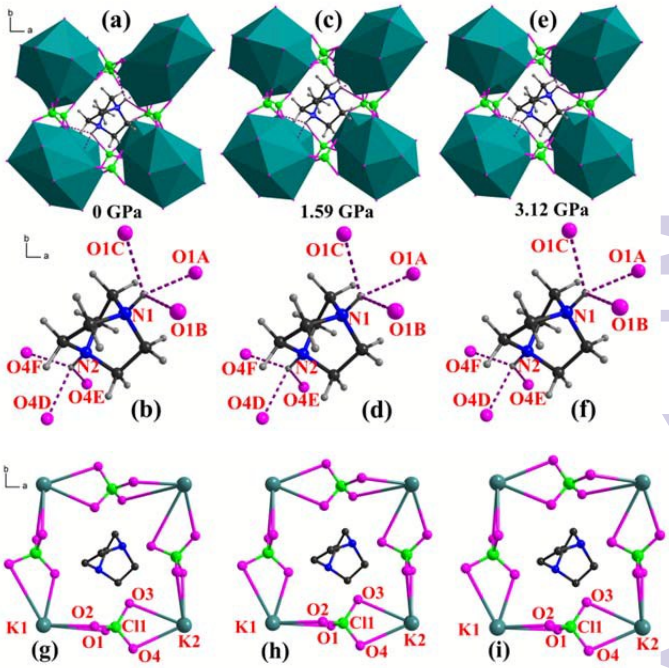

Fig. 1 Framework structure of $[DABCOH_2^{2+}][K(ClO_4)_3]$, the conformation of the $DABCOH_2^{2+}$ cations and the cell unit viewed along the cell axis, at 0 (a,b,g), 1.59 (c,d,h) and 3.12 GPa (e,f,i), refined from DFT based on experimental cell parameters. Colour scheme: K^+, teal; O, pink; Cl, green; C, black; N, blue; H, gray. N–H···O bonds are represented as dashed purple lines, Hydrogen atoms are removed for clarity (g,h,i). Symmetry codes: (A) 0.5+*x, y,* -0.5-*z*; (B) *x,* 0.5-*y,* 0.5+*z*; (C) –*x, -y, -z*; (D) 1+*x, y, z*; (E) -0.5-*x, -y,* 0.5+*z*; (F) 0.5+*x,* 0.5-*y, -z*.

Framework $[DABCOH_2^{2+}][K(ClO_4)_3]$ has an ABX_3 type formula and crystallizes in the cubic space group *Pa*-3 with cell parameters $a = b = c = 14.348(1)$ Å.[12] In the asymmetric unit of the structure, there are two potassium atoms (K1 and K2), a perchlorate ligand (Cl1, O1, O2, O3 and O4) and a $DABCOH_2^{2+}$ cation(Fig.1g). Each K1 atom is coordinated by six O1 atoms and six O2 atoms, while every K2 is surrounded by six O3 atoms and six O4 atoms. Each $K1O_{12}$ polyhedron is connected with six neighboring $K2O_{12}$ polyhedra (and vice versa) *via* the bridging ClO_4^- along three orthogonal directions to form a three-dimensional isotropically packing $[K(ClO_4)_3]^{2-}$ framework (Fig. S1-2). The $DABCOH_2^{2+}$ cation is located in the framework cavity and interacted with the KO_{12} polyhedra *via* two sets of trifurcated N–H···O hydrogen bonds from its two nitrogen ends, namely N(1)-H(1)···O(1) and N(2)-H(2)···O(4) (Fig. 1b). There are four sets of crystalographically indenpendent K-O bonds (K1-O1, K1-O2, K2-O3 and K3-O4), and their bond lengths are listed in Table 1.

Journal Name

ARTICLE

Table 1 Selected bond lengths (Å) and angles (degree) of $[DABCOH_2^{2+}][K(ClO_4)_3]$ at 0, 1.59 and 3.12 GPa, refined *via* DFT using the experimental cell parameters.

Pressure(GPa)	K1-O1	K1-O2	K2-O3	K2-O4	N1···O1	∠N1-H1···O1	N2···O4	∠N2-H2···O4
0	3.5852	2.6884	3.0170	2.8755	2.8797	122.9	2.9770	127.1
1.59	3.3023	2.6926	2.9625	2.8488	2.9149	124.7	2.9627	127.9
3.12	3.2224	2.6759	2.9393	2.8159	2.9017	125.1	2.9360	127.8

Table 2 Summary of the elastic properties of four cubic hybrid crystals. All the elastic tensors are obtained from DFT calculations. The maximal and minimal values of Young's modulus, shear modulus, and Poisson's ratio were determined by using the ElAM software.[23] Anisotropy of *X* is denoted by $A_x = X_{max}/X_{min}$.

Elastic properties	C_{ij} (GPa)			*E* (GPa)		A_E	*G* (GPa)		A_G	*v*		*K* (GPa)
	C_{11}	C_{12}	C_{44}	E_{max}	E_{min}		G_{max}	G_{min}		v_{max}	v_{min}	
MOF-5 (ref.[8])	28.5	12.1	1.7	21.3	4.9	4.3	8.2	1.7	4.8	0.8	0.09	17.6
ZIF-8 (ref.[10])	11.0	8.3	0.9	3.9	2.7	1.4	1.4	0.94	1.5	0.57	0.33	9.2
$CH_3NH_3PbI_3$ (ref.[29])	27.1	11.1	9.2	23.3	20.7	1.1	9.2	8.0	1.2	0.32	0.23	16.4
Framework **1**	40.9	16.3	14.6	36.6	31.6	1.2	14.6	12.3	1.2	0.32	0.20	24.5

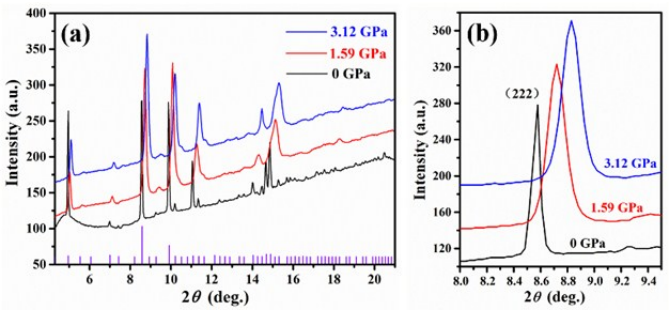

Fig. 2 (a) The representative synchrotron powder diffraction patterns at 0, 1.59 and 3.12 GPa, respectively (Note: the simulated pattern is displayed in the bottom); (b) Shift of the strongest peak (222) with increasing pressure.

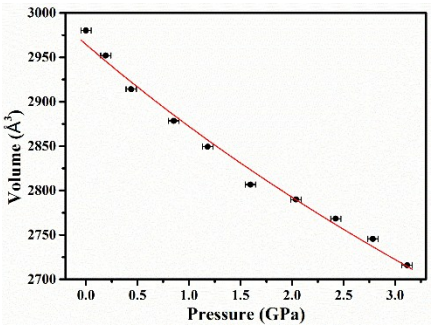

Fig. 3 The evolution of unit cell volume as a function of pressure. The experimental data are shown, with error bars, as black dots, and the red line represents the second-order Birch-Murnaghan fits obtained using PASCal.

The well ground powder of framework $[DABCOH_2^{2+}][K(ClO_4)_3]$ was loaded in a symmetrical DAC for the *in situ* high-pressure PXRD studies. Synchrotron PXRD patterns were collected at different pressures in the range of 0-3.12 GPa, and Fig. 2a shows the representative diffraction patterns at 0, 1.59 and 3.12 GPa. It is apparent that no phase-transition was detected in the whole measured pressure range. As seen in Fig. 2, all the diffraction peaks gradually move to high angles with increasing pressure, which indicates the shrinkage of the whole structure upon compression. The (222) peak is enlarged in Fig. 2b to demonstrate peak broadening in addition to shifting towards to high angle. As pressure increases, some small diffraction peaks disappear and merge with neighbouring bigger ones. However, the crystallinity of framework $[DABCOH_2^{2+}][K(ClO_4)_3]$ is retained in the whole pressure range, which significantly differs from some porous flexible MOFs (i.e. ZIF-8) with low amorphization pressure threshold.[24]

We now focus on the bulk modulus (*K*), which is a measure of volumetric elasticity and represents the resistance of a material against hydrostatic stress. Fig. 3 displays the evolution of the unit cell volume of framework $[DABCOH_2^{2+}][K(ClO_4)_3]$ as a function of pressure. Under hydrostatic conditions, the framework volume contracts about 3% from 0 to 3.12 GPa. The unit cell volume-pressure (*V-P*) data were fitted with second-order Birch-Murnaghan equations of state using PASCal,[25] and the obtained isothermal bulk modulus is 30(1) GPa, which lies in the range of values from dense MOFs (~30-58 GPa)[26] but higher than many known porous MOFs (~5-30 GPa).[27,28] The corresponding axial compressibility (β) is 7.6(4) $\times 10^{-3}$ GPa^{-1}, which indicates that framework $[DABCOH_2^{2+}][K(ClO_4)_3]$ is less compressible than a great deal of porous MOFs but resembles the 'hard' nature of dense MOFs. Notably, the bulk modulus of $[DABCOH_2^{2+}][K(ClO_4)_3]$ is significantly larger than that from the

cubic ZIF-8 (~6.5 GPa),[11] but comparable with those from MOF-5 (~22.3 GPa, between 1.89-2.57 GPa),[29] and cubic phases of hybrid perovskites $CH_3NH_3PbI_3$ (calc. 16.4 GPa).[30]

In order to elucidate the microscopic mechanism of structural changes under pressure, the atomic coordinates of framework $[DABCOH_2^{2+}][K(ClO_4)_3]$ in 0, 1.59 and 3.12 GPa were refined by first-principles geometry optimization based on the experimental cell parameters. Fig. 1 depicts the details of structural evolution from 0, 1.59 to 3.12 GPa, and the selected bond lengths and angle changes are listed in Table 1. With the increase of presure, K1–O2, K2–O3 and K2–O4 bond lengths shrink about 0.5%, 2.1% and 2.6%, respectively. However, the longest K1–O1 bond contracts about 10%, which is almost an order of magnitude higher than those bond contractions under hydrostatic stress from most known MOFs.[27] Notably, the biggest contractions of K1-O1 bonds are linked to the longest bond lengths of 3.5852 Å (0 GPa), 3.3023 Å (1.59 GPa), 3.2224 Å (3.12 GPa). The longer bond length means weaker interaction, so the K1-O1 bonds among four sets of K-O bonds are more likely to deformation under pressure. The compression of K–O bonds induces the flexing of the KO_{12} polyhedra around the cell axis, which then results in the rotation of the perchlorate linker (Fig. 1(g,h,i)). Such structural rearrangement is accompanied by the synergistic variation of the $DABCOH_2^{2+}$ conformation and the host-guest hydrogen bonding. As seen in Fig. 1(b,d,f) and Table 1, the N(1)···O(1) distance and N(1)-H(1)···O(1) angle increase slightly with increasing pressure; while the N(2)···O(4) distance and N(2)-H(2)···O(4) angle show subtle reduction under pressure.

To further understand the comprehensive elastic properties of framework $[DABCOH_2^{2+}][K(ClO_4)_3]$, the full elastic tensors of the optimized crystal structure at 0 GPa were calculated using the DFT-LDA method. The obtained three independent elastic constants are C11 = 40.9, C12 = 16.3 and C44 = 14.6 GPa, respectively (Table 2). The bulk modulus derived from the above calculated elastic tensors is 24.5 GPa, which is in reasonable agreement with the aforementioned synchrotron powder results. The elastic constants C_{ij} and the derived elastic properties, from $[DABCOH_2^{2+}][K(ClO_4)_3]$ and other three known cubic hybrid crystals (MOF-5,[8,9] ZIF-8,[10,11] $CH_3NH_3PbI_3$[24]) are listed in Table 2.

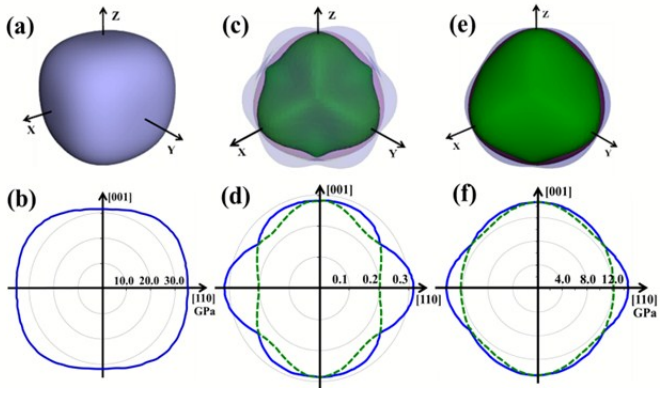

Fig. 4 3D and 2D representations of Young's modulus *E* (a) (b), Poisson's ratio ν (c) (d) and shear modulus *G* (e) (f) for the framework $[DABCOH_2^{2+}][K(ClO_4)_3]$. Color scheme: maximum (blue), minimum positive (green), average positive (purple red).

It is apparent that these C_{ij} for framework $[DABCOH_2^{2+}][K(ClO_4)_3]$ satisfy the following fundamemtal stability criteria required for a cubic crystal: $C_{44}>0$, $C_{11}>|C_{12}|$, $C_{11}+2C_{12}>0$.[31] From Table 2, it can be seen that the calculated C_{11} of framework $[DABCOH_2^{2+}][K(ClO_4)_3]$ is significantly larger than those from porous MOF-5, ZIF-8 and dense $CH_3NH_3PbI_3$. Moreover, C_{12} and C_{44} are the biggest constants among the four tabulated cubic crystals.

The representation surfaces for Young's modulus (*E*) are shown in Fig. 4a, which exhibits deformation sphere with rounded corners, it is clear that Young's modulus for framework $[DABCOH_2^{2+}][K(ClO_4)_3]$ shows a low anisotropy. Due to the fact that C_{44} is smaller than C_{11}, and the contours of *E* are highly distorted along the [001] and [111] directions. *E* reaches the maximum along the <111> body diagonals (E_{max} = 36.6 GPa), and reduces to the minimum for the <100> uniaxial direction (E_{min} = 31.6 GPa), as shown in Fig. 4b. The E_{max} and E_{min} of $[DABCOH_2^{2+}][K(ClO_4)_3]$ are much higher than those from MOF-5 and $CH_3NH_3PbI_3$, and almost an order of magnitude larger than ZIF-8, The anisotropy of elastic modulus, characterized as the ratio $A_E = E_{max}/E_{min}$[32,33] is about 1.2, similar to those from $CH_3NH_3PbI_3$ (1.1) and ZIF-8 (1.4), but significantly lower than the value from MOF-5 (4.3) (Table 2).

For a framework stucture, the elastic and axial deformation are always accompanied by a lateral dimensional change, and this mechanical response is defined as Poisson's ratio $\nu = -e_j/e_i$ (e_j and e_i are the lateral and axial strains, respectively).[21] The 3D and 2D representations of Poisson's ratio (ν) for framework $[DABCOH_2^{2+}][K(ClO_4)_3]$ are shown in Fig. 4(c, d). The calculation gives Poisson's ratio ranging from 0.20 to 0.32, which is significantly narrower than those from MOF-5 and ZIF-8 (Table 2), implying its more isotropic nature in response to axial stretch or compression. For a ductile solid, ν is usually larger than 0.26, which lies in the middle of the ν values of $[DABCOH_2^{2+}][K(ClO_4)_3]$, indicating the boundary nature of $[DABCOH_2^{2+}][K(ClO_4)_3]$ between ductile and brittle. Furthermore, the Poisson's ratio (ν = 0.32) of framework $[DABCOH_2^{2+}][K(ClO_4)_3]$ is maximised when stretched along the <110> direction, which gives rise to a corresponding lateral contraction along the $<1\bar{1}0>$. The Poisson's ratio reaches the minimum (ν = 0.20) with same loading condition accompanied by a lateral contraction along the <001> direction. Such behaviour resembles that of ZIF-8, regardless of their marked structural difference.

Turning attention to the shear modulus (*G*) of framework $[DABCOH_2^{2+}][K(ClO_4)_3]$, the 3D representation surfaces for both the minimal and maximal *G* are shown in Fig. 4(e, f). The maximum shear modulus (*G*) is 14.6 GPa along the <100> direction, the corresponding minimal *G* is 12.3 GPa along the <110> direction. Based on the C_{ij}'s (Table 1), we obtain the defined anisotropy $A = G_{max}/G_{min}$= 1.2, which is in line with the calculation by the Zener's expression $A' = 2C_{44}/(C_{11} - C_{12})$.[34] Specifically, in Zener's defintion, for a single crystal with cubic symmetry the elastic anisotropy index can be characterized by A' coefficient, C_{44} represents resistance to a shear in the {100} plane along the <0kl> direction, while $C' = (C_{11}-C_{12})/2$ represents resistance to a shear in the {110} plane along the $<1\bar{1}0>$ direction. Here, for framework $[DABCOH_2^{2+}][K(ClO_4)_3]$, $G_{max} = C_{44}$

= 14.6 GPa and G_{min} = C′ = 12.3 GPa are derived from the C_{ij}'s (Table 2). These values are significantly larger than those from MOF-5 and $CH_3NH_3PbI_3$, and more than an order of magnitude higher than ZIF-8. The high shear moduli of $[DABCOH_2^{2+}][K(ClO_4)_3]$ indicate its much better stability against structural deformation compared with MOF-5, ZIF-8 and $CH_3NH_3PbI_3$, which could be an advantage in the industrial manufacturing and processing for structurally similar frameworks with desired functionalities.

Overall, framework $[DABCOH_2^{2+}][K(ClO_4)_3]$ exhibits more isotropic elastic properties compared with MOF-5, ZIF-8 and many other MOFs, which could be explained by the following reasons. First of all, the considerably large coordination number of KO_{12} polyhedra respond more isotropically compared with common metal octahedra or tetrahedra under stress; secondly, the pyrimidal perchlorate ligands give rise to less anisotropic deformation against mechanical perturbation in contrast to many linear ligands.[27]

Conclusions

In this contribution, we have studied the hydrostatic behaviour of a dense hybrid framework, $[DABCOH_2^{2+}][K(ClO_4)_3]$, *via* synchrotron X-ray powder diffraction between 0-3.12 GPa. This study has demonstrated that this material contracts about 3% in terms of volume, in the studied pressure range. Data fitting, using the second-order Birch-Murnaghan equations of state, gives bulk modulus and linear compressibility of 30(1) GPa and $7.6(4)\times10^{-3}$ GPa^{-1}. The contraction mechanism is initiated by the shrinkage of the K–O bonds within the KO_{12} polyhedra, which induces the rotation of the perchlorate anions and cooperative movement of the $DABCOH_2^{2+}$cations.

In addition, we have calculated the full elastic tensors of framework $[DABCOH_2^{2+}][K(ClO_4)_3]$ by first-principles calculations, and the derived Young's moduli, shear moduli, Poisson's ratios are extensively analysed. We found that the Young's and shear moduli of [DABCOH22+][K(ClO4)3] are much higher than those from MOF-5 and CH3NH3PbI3, and about an order of magnitude larger than ZIF-8. Furthermore, the Poisson's ratios of [DABCOH22+][K(ClO4)3] have a very narrow range, which indicates this materials' isotopic nature in response to axial stretching or compressing. The values of Poisson's ratios in [DABCOH22+][K(ClO4)3] also indicate that it could be between ductile and brittle. To finish, this study has given one more example about the better understanding of mechanical properties of dense hybrid framework materials. And the high mechanical strength of these frameworks indicates that their more robust nature against stress could be an advantage in the future industrial manufacturing and processing.

Acknowledgements

G.F., W.W. and W.L. acknowledge funding support from the Opening Project of the Key Laboratory of Cryogenics in the Technical Institute of Physics and Chemistry, Chinese Academy of Sciences, Huazhong University of Science and Technology and National Natural Science Foundation of China (Grant No.61138006 and 21571072).

Notes and reference

1 A. K. Cheetham, C. N. R. Rao, R. K. Feller, Chem. Commun., 2006, 4780.
2 S. Kitagawa, R. Kitaura, S. Noro, Angew. Chem. Int. Ed., 2004, 43, 2334.
3 P. Docampo, J. M. Ball, M. Darwich, G. E. Eperon , H. J. Snaith, Nature Commun., 2013, 4, 2761.
4 Z. K. Tan, R. S. Moghaddam, M. L. Lai, P. Docampo, R. Higler, F. Deschler, M. Price, A. Sadhanala, L. M. Pazos, D. Credgington, F. Hanusch, T. Bein, H. J. Snaith, R. H. Friend, Nature Nanotech., 2014, 9, 687.
5 Z. Y. Zhang, W. Li, M. A. Carpenter, C. J. Howard, A. K. Cheetham, CrystEngComm., 2015, 17, 370.
6 G.-C. Xu, X.-M. Ma, L. Zhang, Z.-M. Wang, S. Gao, J. Am. Chem. Soc. 2010, 132, 9588.
7 W. Li, M. R. Probert, M. Kosa, T. D. Bennett, A. Thirumurugan, R. P. Burwood, M. Parinello, J. A. K. Howard, A. K. Cheetham, J. Am. Chem. Soc. 2012, 134, 11940.
8 D. F. Bahr, J. A. Reid, W. M. Mook, C. A. Bauer, R. Stumpf, A. J. Skulan, N. R. Moody, B. A. Simmons, M. M. Shindel, M. D. Allendorf, Phys. Rev. B, 2007, 76, 184106.
9 J. A. Greathouse, M. D. Allendorf, J. Phys. Chem. C., 2008, 112, 5795.
10 J. C. Tan, B. Civalleri, C. C. Lin, L. Valenzano, R. Galvelis, P. F. Chen, T. D. Bennett, C. M. Draznieks, C. M. Z. Wilson, A. K. Cheetham, Phys. Rev. Lett., 2012, 108, 095502.
11 K. W. Chapman, G. J. Halder, P. J. Chupas, J. Am. Chem. Soc., 2009, 131, 17546.
12 Z. M. Jin, Y. J. Pan, X. F. Li, M. L. Hu, L. Shen, J. Mol. Struct., 2003, 660, 67.
13 H. K. Mao, J. Xu, P. M. Bell, J. Geophys. Res., 1986, 91, 4673.
14 J. Hammersley, Fit2d User Manual. 1996.
15 B. H. Toby, J. Appl. Crystallogr., 2001, 34, 210.
16 S. J. Clark, M. D. Segall, C. J. Pickard, P. J. Hasnip, M. J. Probert, K. Refson, M. C. Payne, Z. Kristallogr., 2005, 220, 567.
17 M. C. Payne, M. P. Teter, D. C. Allan, T. A. Arias, J. D. Joannopoulos, Rev. Mod. Phys., 1992, 64, 1045.
18 (a) J. P. Perdew, A. Zunger, Phys. Rev. B., 1981, 23, 5048; (b) D. M. Ceperley, B. J. Alder, Phys. Rev. Lett. 1980, 45, 566.
19 A. M. Rappe, K. M. Rabe, E. Kaxiras, J. D. Joannopoulos, Phys. Rev. B., 1990, 41, 1227.
20 H. J. Monkhorst, J. D. Pack, Phys. Rev. B., 1976, 13, 5188.
21 B. G. Pfrommer, M. Cote, S. G. Louie, M. L. Cohen, J. Comput. Phys., 1997, 131, 233.
22 (a) C. J. Pickard, R. J. Needs, Nat. Mater., 2010, 9, 624; (b) C. J. Pickard, R. J. Needs, Nat. Mater., 2008, 7, 775.
23 A. Marmier, Z. A. D. Lethbridge, R. I. Walton, C. W. Smith, S. C. Parker, K. E. Evans, Compu. Phys. Commun., 2010, 181, 2102.
24 (a) K. W. Chapman, D. F. Sava, G. J. Halder, P. J. Chupas, T. M. Nenoff, J. Am. Chem. Soc., 2011, 133, 18583–18585; (b) K. W. Chapman, G. J. Halder, P. J. Chupas, J. Am. Chem. Soc., 2009, 131, 17546.
25 M. J. Cliffe, A. L. Goodwin, J. Appl. Cryst., 2012, 45, 1321.
26 (a) E. C. Spencer, N. L. Ross, R. J. Angel, J. Mater. Chem. 2012, 22, 2074; (b) E. C. Spencer, M. S. R. N. Kiran, W. Li, U. Ramamurty, N. L. Nancy, A. K. Cheetham, Angew. Chem. Int. Edit., 2014, 53, 5583; (c) M. Zhou, K. Wang,

Z. Men, C. Sun, Z. Li, B. Liu, G. Zou and B. Zou, CrystEngComm, 2014, 16, 4084.
27 J. C. Tan, A. K. Cheetham, Chem. Soc. Rev., 2011, 40, 1059.
28 (a) J. C. Tan, B. Civalleri, A. Erba，E. Albanese, CrystEngComm., 2015, 17, 375. (b) M. R. Ryder, J. C. Tan, Dalton Trans., 2016, **DOI:** 10.1039/c5dt03514g.
29 A. J. Graham, D. R. Allan, A. Muszkiewicz, C. A. Morrison, S. A. Moggach, Angew. Chem. Int. Ed. 2011, 50, 11138.
30 J. Feng, APL Mater., 2014, 2, 081801.
31 J. F. Nye, Physical Properties of Crystals., Clarendon press, Oxford, 1985, pp. 142.
32 B. Amadei, Int. J. Rock Mech. Min. Sci & Geomech.Abstr, 1996, 33, 293.
33 G. Worotnicki，In Comprehensive Rock Engineering, Pergamon, Oxford, 1993, pp. 329.
34 C. Zener, Elasticity and Anelasticity of Metals., University of Chicago press, Chicago, 1948, pp. 16.